Critical Transport and Vortex Dynamics in a Thin Atomic Josephson Junction

K. Xhani,[1,2] E. Neri,[3] L. Galantucci,[1] F. Scazza,[2,4] A. Burchianti,[2,4] K.-L. Lee,[1] C. F. Barenghi,[1] A. Trombettoni,[5] M. Inguscio,[2,4,6] M. Zaccanti,[2,3,4] G. Roati,[2,4] and N. P. Proukakis[1]

[1]*Joint Quantum Centre (JQC) Durham-Newcastle, School of Mathematics, Statistics and Physics, Newcastle University, Newcastle upon Tyne NE1 7RU, United Kingdom*

[2]*European Laboratory for Non-Linear Spectroscopy (LENS), Università di Firenze, 50019 Sesto Fiorentino, Italy*

[3]*Dipartimento di Fisica e Astronomia, Università di Firenze, 50019 Sesto Fiorentino, Italy*

[4]*Istituto Nazionale di Ottica del Consiglio Nazionale delle Ricerche (CNR-INO), 50019 Sesto Fiorentino, Italy*

[5]*CNR-IOM DEMOCRITOS Simulation Center and SISSA, Via Bonomea 265, I-34136 Trieste, Italy*

[6]*Department of Engineering, Campus Bio-Medico University of Rome, 00128 Rome, Italy*

(Received 20 May 2019; published 31 January 2020)

We study the onset of dissipation in an atomic Josephson junction between Fermi superfluids in the molecular Bose-Einstein condensation limit of strong attraction. Our simulations identify the critical population imbalance and the maximum Josephson current delimiting dissipationless and dissipative transport, in quantitative agreement with recent experiments. We unambiguously link dissipation to vortex ring nucleation and dynamics, demonstrating that quantum phase slips are responsible for the observed resistive current. Our work directly connects microscopic features with macroscopic dissipative transport, providing a comprehensive description of vortex ring dynamics in three-dimensional inhomogeneous constricted superfluids at zero and finite temperatures.

DOI: 10.1103/PhysRevLett.124.045301

Interest is growing in model systems that allow for investigating the interplay between resistive and dissipationless quantum transport phenomena. In this context, ultracold gases in tailored optical potentials represent an ideal framework, owing to the real-time control over the relevant parameters in experiments [1,2], combined with the ability for *ab initio* modeling [3,4]. A paradigmatic example is the study of the dynamics between two atomic superfluids weakly coupled through a thin tunneling barrier. This realizes a Josephson junction [5,6], which represents a minimal platform to observe both coherent quantum transport [6,7], and its breakdown driven by dissipative microscopic mechanisms [8,9].

The coherent dynamics of atomic Josephson junctions (JJs) [10–20] is governed by the competition between the charging energy E_C and the Josephson tunneling energy E_J [10,11]. E_C relates the chemical potential difference across the tunneling barrier to the relative population imbalance between the reservoirs, and depends on interparticle interactions. E_J promotes the delocalization of the superfluid across the two reservoirs and sets the maximum coherent flow through the weak link. When E_J dominates, superfluid current and relative phase oscillate in quadrature at the Josephson plasma frequency. In the opposite regime, and in the absence of dissipation [11,12], the system may enter the Macroscopic Quantum Self-Trapping (MQST) regime. This is characterized by high-frequency coherent oscillations of the population imbalance around a nonzero value, driven by a monotonically increasing relative phase [10,13,15–18]. Even without thermally induced decay of the population imbalance [12,17,21], the stability of MQST depends on whether vortices nucleated inside the barrier annihilate therein [22,23], or penetrate into the superfluid reservoirs. Recent experiments with inhomogeneous three-dimensional Fermi superfluids [24,25] revealed the intimate connection between phase slippage and dissipation arising from vortices created within the barrier and shed into the superfluid. Similar effects have been studied in ring-shaped bosonic condensates [26–29], mesoscopic structures [30,31], and lower-dimensional geometries [32–34]. While vortices crossing the weak link are known to yield a finite resistance [25,27,30], the relation between microscopic vortex nucleation, dynamics, and macroscopic dissipative flow is still poorly understood.

In this work we demonstrate the connection between resistive superfluid currents and vortex ring (VR) dynamics in an atomic JJ of fermionic superfluids. We obtain the critical population imbalance and the maximum coherent current delimiting the boundary between dissipationless and dissipative transport even at finite temperatures. We find excellent agreement with recent measurements [24,25], thus clarifying their interpretation. Trap asymmetry is shown to foster the emergence of elliptical VRs exhibiting Kelvin-wave excitations, while thermal fluctuations reduce the VR lifetime.

Methodology.—Our numerical simulations are based on the experimental parameters of Ref. [25]. We consider two molecular Bose-Einstein condensates (BECs) of about 10^5 atom pairs of ^{6}Li, weakly coupled through a thin optical barrier, at $1/k_F a \sim 4.6$ (where k_F is the Fermi wave vector and a the interatomic scattering length). The harmonic trapping potential is asymmetric with approximately (1:12:10) ratio along the x, y, and z axis, respectively. The Gaussian barrier bisects the gas along the weakest (x) direction (with $\nu_x = 15$ Hz), with a $1/e^2$ waist, $w \sim 4\xi$, where ξ is the superfluid coherence length [25]. The superfluid transport through the barrier is triggered by an initial nonzero population imbalance $z_0 = z_{\rm BEC}(0)$ between the two reservoirs. Here, $z_{\rm BEC}(t) = [N_R(t) - N_L(t)]/N_{\rm BEC}$, with $N_L(N_R)$ the BEC number in the left (right) reservoir, and $N_{\rm BEC} = N_L + N_R$ the total condensate number. The imbalance corresponds to a chemical potential difference $\Delta\mu = \mu_L - \mu_R = E_C z_0 N_{\rm BEC}/2$. Dynamics in the $T = 0$ limit are simulated via the time-dependent Gross-Pitaevskii equation (GPE), extended to nonzero temperatures $T \lesssim 0.4 T_c$ (where T_c is the BEC critical temperature), via its coupling to a collisionless Boltzmann equation [3,35,36]. We stress that the standard two-mode model [10,13] that captures both Josephson and MQST dynamics of previous experiments [16,18] is out of its validity range due to the considered values of the ratio V_0/μ and to the thinness of the junctions [36]. Although dissipative effects can be *phenomenologically* modeled by damped two-mode [21,57,58] and RSJ-circuital models [7], such approaches provide limited insight into the microscopic dissipative processes.

Dynamical regimes and phase diagram.—We study $z_{\rm BEC}(t)$, varying both the initial population imbalance z_0 and the barrier height V_0. At each value of V_0 we observe two distinct dynamical regimes. For z_0 smaller than a critical value $z_{\rm cr}$, $z_{\rm BEC}(t)$ exhibits sinusoidal plasma oscillations (Josephson regime). For $z_0 \geq z_{\rm cr}$, we instead observe an initial rapid decay of $z_{\rm BEC}(t)$ (dissipative regime), followed by plasma oscillations with amplitude smaller than $z_{\rm cr}$. We validate our numerics by comparing $z_{\rm BEC}(t)$ with experiments under the same conditions, finding excellent agreement [Fig. 1(a), insets]. Combining calculated and newly extracted experimental $z_{\rm cr}$ values, we map out the phase diagram delimiting Josephson and dissipative regimes as a function of the normalized barrier height $V_0/\mu(T)$ [Fig. 1(a)], where $\mu(T)$ is the chemical potential including the thermal mean-field contribution [35,36]. Increasing $V_0/\mu(T)$, the onset of dissipation appears at smaller $z_{\rm cr}$. This reproduces the observed boundary within experimental uncertainty up to $T \approx 0.3 T_c$ upon keeping the *condensate* number equal to the $T = 0$ case. Our findings can also be interpreted in terms of the critical current $I_{\rm max}$ across the junction, defined as the maximum value of $I = \dot{z}_{\rm BEC} N_{\rm BEC}/2$ at $z_0 = z_{\rm cr}$ [Fig. 1(b)]. Numerically, $|I|_{\rm max}$ is well approximated by $z_{\rm cr}\omega_J N_{\rm BEC}/2$, where ω_J is the Josephson plasma frequency. The corresponding $|I|_{\rm max}$ from the experimentally determined $z_{\rm cr}$ and ω_J is in excellent agreement with the theoretical prediction. The overall trend of $|I|_{\rm max}$ against $V_0/\mu(T)$ is also quantitatively captured by extending to inhomogeneous systems an analytical model, originally developed for two homogeneous BECs weakly coupled through a rectangular barrier [20,36,59].

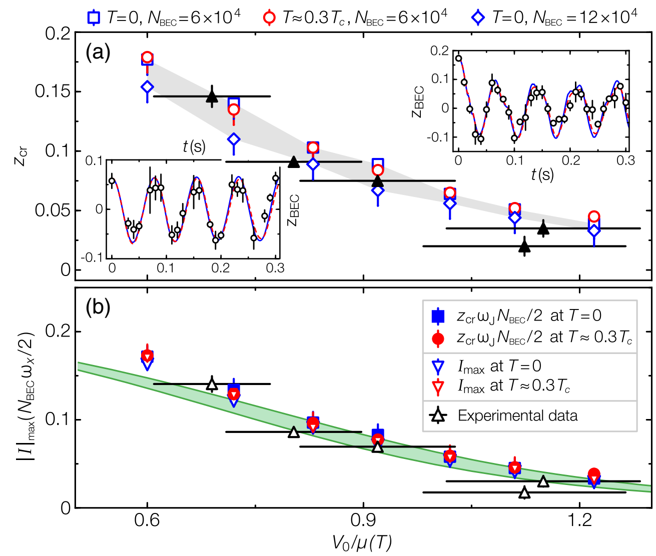

FIG. 1. Phase diagram of a thin Josephson junction: (a) Critical population imbalance $z_{\rm cr}$ as a function of $V_0/\mu(T)$, via numerical simulations at $T = 0$ (blue symbols) and $T \approx 0.3 T_c$ (red circles), and experimental data (black triangles). Grey shaded area accounts for the experimental range of particle number. Vertical error bars are set by the discreteness of the numerically probed z_0 values (simulations) and the standard deviations over at least four measurements (experiments); horizontal experimental error bars are set by the combined uncertainties in measuring barrier width, particle number, and laser power. Insets: Comparison of numerical (blue and red lines) and experimental population imbalance evolution in Josephson (left) and dissipative (right) regimes. (b) Maximum superfluid current, $|I|_{\rm max}$, based on the numerical time derivative of population imbalance (down triangles), and on the numerical and experimental estimate $|I|_{\rm max} \simeq z_{\rm cr}\omega_J N_{\rm BEC}/2$. Green shaded area: Predicted maximum supercurrent (including second-order harmonics in the current-phase relation), accounting for the uncertainty in V_0/μ [36].

Vortex ring nucleation and evolution.—The onset of the dissipative regime for $z_0 \geq z_{\rm cr}$ in [24,25] has been linked to the appearance of topological defects in the superfluid. Here, we fully characterize such dynamical features at $T = 0$, by computing the superfluid velocity $\mathbf{v} = (\hbar/M)\nabla\phi$, where M is the atom pair mass and ϕ the condensate phase (see later for thermal effects). Given the symmetry of our junction, we consider the x component of the superfluid velocity, weighted over the transverse density in the $x = 0$ plane, $\langle v_x \rangle$ [36]; we identify three distinct dynamical stages (I, II, and III, see Fig. 2) in the nucleation process of the first VR (the emerging pattern applies to subsequent VRs). In stage I, following the Josephson-Anderson relation $M\dot{\mathbf{v}} = -\nabla\mu$ [60–62], the

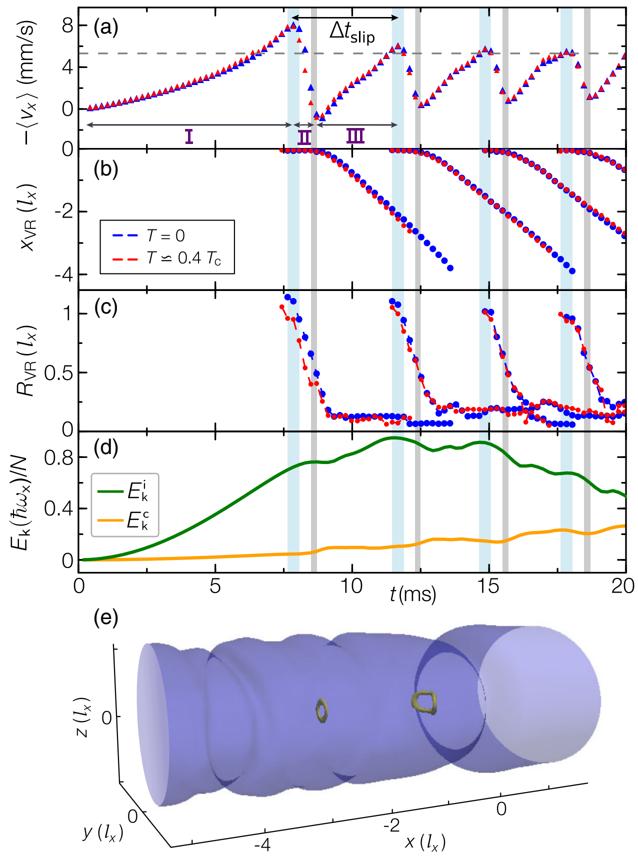

FIG. 2. Vortex ring generation and early-stage dynamics. (a) Density-weighted x component of superfluid velocity at the barrier (dashed line denotes mean speed of sound $\langle c \rangle = \sqrt{\mu/2M}$). (b) Mean radius and (c) position of the first few generated vortex rings (units of $l_x = \sqrt{\hbar/M\omega_x}$). (d) Temporal evolution of the incompressible (E_k^i) and compressible (E_k^c) kinetic energy of the BEC. Vertical shaded blue areas denote the maxima of superfluid velocity when VRs are generated, while grey areas indicate the times when the VRs enter the Thomas-Fermi surface. Shown are both $T = 0$ (blue symbols) and $T \approx 0.4T_c$ (red symbols) for $z_0 = 0.25$, $V_0/\mu \simeq 0.8$ and $N_{\rm BEC} \simeq 6 \times 10^4$. (e) BEC density isosurface at 19.5 ms, when the third and fourth VRs are visible.

chemical potential gradient $\nabla\mu$ drives a unidirectional, accelerated superfluid flow across the junction. When $-\langle v_x \rangle$ reaches a critical value exceeding the mean sound speed $\langle c \rangle$ [Fig. 2(a)], a VR is nucleated, associated with a relative-phase jump of 2π [36]. It originates outside the Thomas-Fermi (TF) surface on the central radial plane, $x = 0$, where, the superfluid velocity is maximum, due to the flow constriction, and the local speed of sound is minimum, since density vanishes. After its nucleation [stage II], the VR moves axially very slowly away from its nucleation region $x_{\rm VR} = 0$ [Fig. 2(b)] with its mean radius $R_{\rm VR}$ rapidly shrinking [Fig. 2(c)] due to the strong radial density inhomogeneity in the barrier region, until it is comparable to the transversal TF radius of the BEC, and enters the bulk superfluid [22]. During such evolution, $-\langle v_x \rangle$ exhibits a rapid decrease, possibly even changing sign. Then, in stage III, the VR gradually leaves the barrier region with the axial velocity $-\langle v_x \rangle$ reaccelerated by $\nabla\mu$ [Fig. 2(a)], until some time later ($\Delta t_{\rm slip} \simeq h/\Delta\mu$), when it has already traveled a considerable distance from the barrier edge, another VR is nucleated at the trap center [see, e.g., Fig. 2(e)]. Note that early on in stage III, before the VR exits the barrier region (i.e., before reaching the point of maximum transversal TF radius), $R_{\rm VR}$ continues decreasing due to the strong background density gradient.

For a deeper insight into the underlying superfluid dynamics, we decompose at $\mathbf{x} = \mathbf{0}$ the total axial superfluid velocity $v_x = v_f + v_\omega$, where v_f is the main flow velocity (which is slowly varying compared to the timescale of the early vortex dynamics) and v_ω is the VR-generated swirling velocity [36]; we also initially neglect compressibility effects (addressed in the next paragraph). By the end of stage II, the shrinking VR has just left the trap center, and so the vortex contribution v_ω evaluated at $\mathbf{x} = \mathbf{0}$ (where the local superfluid velocity $\langle v_x \rangle$ shown in Fig. 2(a) is calculated) tends to 0. This leads to a drop of $\langle v_x \rangle$ with amplitude $\Delta\langle v_x \rangle \sim \kappa/R_{\rm VR}$, corresponding to the change in the axial superfluid velocity at the trap center due to the lost vortex contribution, where κ is the quantum of circulation [36]. This sawtoothlike profile of $\langle v_x \rangle$ [Fig. 2(a)] is typical of phase slippage phenomena seen in superfluid helium [60–63], with the less abrupt drop found here stemming from the initial persistence of the VR within the barrier region.

The drop $\Delta\langle v_x \rangle$ can even overcome the generating flow velocity, leading to flow reversal (i.e., backflow) in the postnucleation dynamics, in agreement with Biot-Savart calculations [36]. The amplitude of each subsequent velocity drop is reduced due to the overall decay of $z_{\rm BEC}(t)$.

To connect the dissipation with the microscopic VR nucleation and dynamics, and phonon emission, we decompose the temporal evolution of the BEC total kinetic energy in its incompressible E_k^i, compressible E_k^c, and quantum pressure E_q contributions [36,64]. E_k^i and E_k^c correspond respectively to the kinetic energy of the flow (both potential flow driven by $\nabla\mu$ and vortex generated swirls) and to the sound wave energy in the superflow. E_q accounts for the energy arising from density inhomogeneities due to the trapping potential [36]. When each VR enters the TF surface (end of stage II), and while still propagating within the barrier's region of increasing density, sound waves are emitted and E_k^c increases at the expenses of E_k^i [Fig. 2(d)] [36]. The dissipation of Josephson oscillations [25,60–62] thus stems from two effects: the incompressible kinetic energy transferred from the axial flow to the vortex swirling flow and the phonon emission occurring during vortex nucleation and propagation within the barrier region.

We further quantify both those effects by considering the effect of z_0 on the velocity $v_{\rm VR}$ and the incompressible

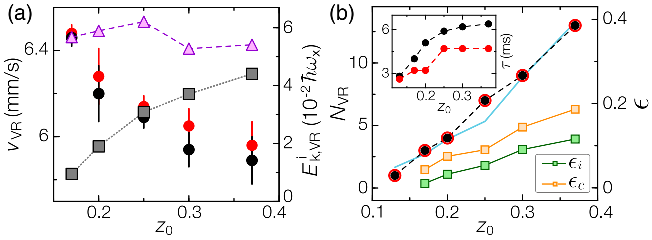

FIG. 3. Role of initial population imbalance z_0 (for fixed $V_0/\mu \simeq 0.8$ for which $z_{cr} \simeq 0.11$) on: (a) velocity v_{VR} (left axis, red and black circles) and incompressible kinetic energy $E^i_{k,\mathrm{VR}}$ (right axis, grey squares) of first nucleated VRs. Pink triangles indicate the VR energy calculated with the analytical formula for homogeneous unbounded BECs [36]; (b) total number N_{VR} of VRs penetrating the bulk (left axis, circles) and vortex induced dissipations ϵ_i and ϵ_c (right axis, green and yellow squares). Blue line connects N_{VR} estimates from the time-averaged phase-slippage rate $\Delta\mu(t)/h$ [60]. Inset: Lifetimes, τ, of first nucleated VRs. Each subplot shows $T = 0$ (black symbols) and $T \approx 0.4T_c$ (red symbols) results.

kinetic energy $E^i_{k,\mathrm{VR}}$ of the first VR nucleated; this is shown in Fig. 3 for $z_0 \in [0.13, 0.37]$ and $V_0/\mu = 0.8$. We find that increasing z_0 leads to a decreasing v_{VR} and to a monotonic increase of $E^i_{k,\mathrm{VR}}$ [Fig. 3(a)] [36]. Calculating the fraction of the total kinetic energy flowing through the junction until the nucleation of the first VR which is dissipated in sound (ϵ_c) or transferred to the first VR (ϵ_i) [36], we find that both sources of dissipation increase as z_0 gets larger [see Fig. 3(b)], and can cumulatively account for a significant fraction of the total energy. Surprisingly, the acoustic dissipation ϵ_c is always larger than the incompressible contribution ϵ_i. Increasing z_0 leads to more nucleated vortices N_{VR} [Fig. 3(b)], due to the larger time-averaged chemical potential difference [60], consistent with Ref. [25] and with earlier studies of controlled vortex generation [65,66]. Similarly, the VR lifetime increases by increasing z_0 [Fig. 3(b) (inset)]. The VR survival during its propagation in the superfluid bulk is thus determined by two competing effects: On the one hand, the VR tends to expand [67] to conserve its incompressible kinetic energy as it moves towards lower-density regions with decreasing transverse size. On the other hand, the radial trapping asymmetry ($\omega_y \neq \omega_z$) leads to elliptical VR profiles with oscillating aspect ratio, corresponding to a $m = 2$ Kelvin-wave excitation on a circular VR [68]. This wobbling motion induces dissipation of the VR incompressible kinetic energy via the emission of phononlike excitations, reducing the VR radius [69,70]: When $R_{\mathrm{VR}} \sim \xi$, the VR loses its circulation and annihilates in a rarefaction pulse [22].

This picture remains qualitatively correct for the probed $T \lesssim 0.4T_c$ (red symbols in Figs. 2–3), for which no thermal VR activation occurs ($k_B T < 0.8V_0$). For a fixed BEC number, superfluid flow, VR generation, and early dynamics are not noticeably affected by the thermal cloud, whose main effect is to add an extra potential to the BEC [35,36,71–73]. Over longer timescales, dissipation due to relative BEC-thermal motion becomes relevant, decreasing the VR lifetime [Fig. 3(b)].

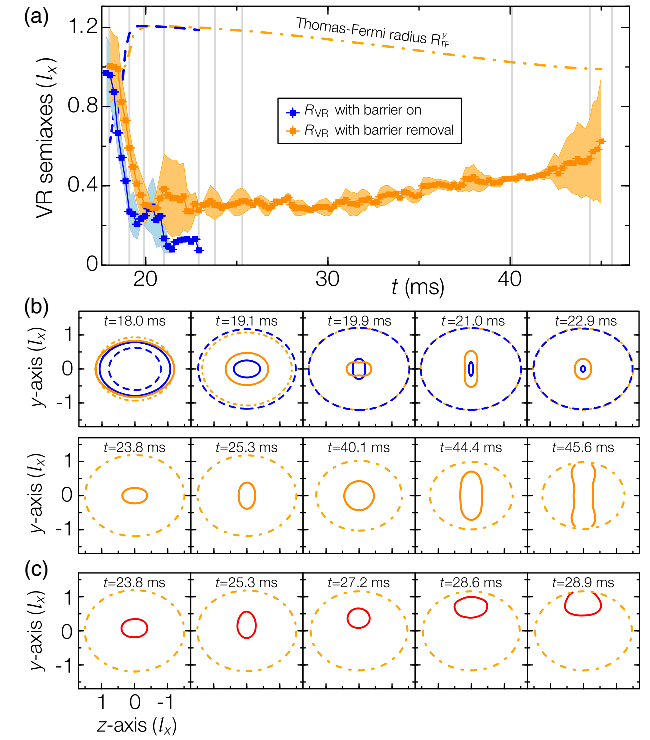

FIG. 4. Vortex ring evolution under different conditions: (a) Evolution of the semiaxes and mean radius of the fourth VR ($z_0 = 0.25$, $V_0/\mu \simeq 0.8$), with barrier kept on (blue line) or removed during [13,53] ms (orange line). Shadowed areas mark limiting values of the two semiaxes. Dashed blue and orange lines on top: Transverse TF radius at the instantaneous VR location. (b) Dynamical 2D VR profiles with barrier on (blue) and removed (orange) plotted alongside the corresponding transverse TF surface (dash-dotted lines). Displayed profiles correspond to evolution times marked by vertical solid lines in (a), with the VR surviving only until $t \simeq 23$ ms with barrier on. (c) Typical evolution of a 2D VR profile in the case of barrier removal at $T \approx 0.4T_c$. The VR moves off axis, generating a single vortex handle at the boundary.

To connect with Refs. [24,25], we implement in our simulations the same protocol by which vortices were observed in time of flight after gradually removing the barrier with a 40 ms linear ramp. The dynamics of the fourth VR generated in the same conditions as in Fig. 2 [right VR in Fig. 2(e)] is shown in Fig. 4, including or excluding the barrier removal procedure. Upon removing the barrier (orange curve), the VR propagates for longer time and longer distance [Fig. 4(a)]. This facilitates the direct observation of Kelvin-wave oscillations [visible in Fig. 4(b)], whose period is consistent with the dispersion relation $\omega(k) \sim \kappa k^2/(4\pi)[\ln(2/(k\xi) - 0.5772]$ [36,68]. The longer lifetime can be attributed to the larger kinetic energy of VRs nucleated during the gradual barrier removal process. As the VR approaches the edge of the condensate, it breaks up into two antiparallel vortex lines [Fig. 4(b), final snapshot] [22,67,74]. Critically, thermal fluctuations destabilize the VR, causing it to drift off axis, and reach the transversal boundary asymmetrically [Fig. 4(c)] (see also Ref. [75]). There, it reconnects with its image and forms a "vortex handle" [76–78]. This could explain why a single vortex line is typically detected in each experimental run after barrier removal [24,25].

Conclusions.—We have studied the complex interplay between coherent and dissipative dynamics in a thin atomic Josephson junction. We have shown that resistive currents are directly connected with nucleations of vortex rings and their propagation into the superfluid bulk. In particular, dissipation originates from two irreversible effects: phonon emission when vortex rings are nucleated, and incompressible kinetic energy transfer from the superfluid flow to the swirling one of the nucleated vortex rings. The detailed understanding of the connection between vortex-ring dynamics and dissipation is valuable for advancing our comprehension of the complex superfluid dynamics in emerging atomtronic devices [79].

Data supporting this publication is openly available under an Open Data Commons Open Database License [80].

We thank A. Smerzi and A. Muñoz Mateo for valuable discussions. This work was supported by QuantERA project NAQUAS (EPSRC EP/R043434/1), EPSRC project EP/R005192/1, Fondazione Cassa di Risparmio di Firenze project QuSim2D 2016.0770, European Research Council Grant Agreements No. 307032 QuFerm2D and No. 637738 PoLiChroM, and European Union's Horizon 2020 research and innovation programme under the Marie Skłodowska-Curie Grant Agreement No. 705269.

[1] C.-C. Chien, S. Peotta, and M. Di Ventra, Nat. Phys. **11**, 998 (2015).

[2] S. Krinner, T. Esslinger, and J.-P. Brantut, J. Phys. Condens. Matter **29**, 343003 (2017).

[3] *Quantum Gases: Finite Temperature and Non-Equilibrium Dynamics*, edited by N. Proukakis, S. Gardiner, M. Davis, and M. Szymańska (Imperial College Press, London, United Kingdom, 2013).

[4] N. G. Berloff, M. Brachet, and N. P. Proukakis, Proc. Natl. Acad. Sci. U.S.A. **111**, 4675 (2014).

[5] B. D. Josephson, Phys. Lett. **1**, 251 (1962).

[6] A. Barone and G. Paternò, *Physics and Applications of the Josephson Effect* (John Wiley, New York, 1982).

[7] M. Tinkham, *Introduction to Superconductivity*, 2nd ed. (McGraw-Hill, New York, 1996).

[8] A. Caldeira and A. Leggett, Ann. Phys. (N.Y.) **149**, 374 (1983).

[9] R. Fazio and H. van der Zant, Phys. Rep. **355**, 235 (2001).

[10] A. Smerzi, S. Fantoni, S. Giovanazzi, and S. R. Shenoy, Phys. Rev. Lett. **79**, 4950 (1997).

[11] I. Zapata, F. Sols, and A. J. Leggett, Phys. Rev. A **57**, R28 (1998).

[12] J. Ruostekoski and D. F. Walls, Phys. Rev. A **58**, R50 (1998).

[13] S. Raghavan, A. Smerzi, S. Fantoni, and S. R. Shenoy, Phys. Rev. A **59**, 620 (1999).

[14] F. S. Cataliotti, S. Burger, C. Fort, P. Maddaloni, F. Minardi, A. Trombettoni, A. Smerzi, and M. Inguscio, Science **293**, 843 (2001).

[15] T. Anker, M. Albiez, R. Gati, S. Hunsmann, B. Eiermann, A. Trombettoni, and M. K. Oberthaler, Phys. Rev. Lett. **94**, 020403 (2005).

[16] M. Albiez, R. Gati, J. Fölling, S. Hunsmann, M. Cristiani, and M. K. Oberthaler, Phys. Rev. Lett. **95**, 010402 (2005).

[17] S. Levy, E. Lahoud, I. Shomroni, and J. Steinhauer, Nat. Phys. **449**, 579 (2007).

[18] G. Spagnolli, G. Semeghini, L. Masi, G. Ferioli, A. Trenkwalder, S. Coop, M. Landini, L. Pezzè, G. Modugno, M. Inguscio, A. Smerzi, and M. Fattori, Phys. Rev. Lett. **118**, 230403 (2017).

[19] L. J. LeBlanc, A. B. Bardon, J. McKeever, M. H. T. Extavour, D. Jervis, J. H. Thywissen, F. Piazza, and A. Smerzi, Phys. Rev. Lett. **106**, 025302 (2011).

[20] F. Meier and W. Zwerger, Phys. Rev. A **64**, 033610 (2001).

[21] Y. M. Bidasyuk, M. Weyrauch, M. Momme, and O. O. Prikhodko, J. Phys. B **51**, 205301 (2018).

[22] F. Piazza, L. A. Collins, and A. Smerzi, New J. Phys. **13**, 043008 (2011).

[23] M. Abad, M. Guilleumas, R. Mayol, F. Piazza, D. M. Jezek, and A. Smerzi, Europhys. Lett. **109**, 40005 (2015).

[24] G. Valtolina, A. Burchianti, A. Amico, E. Neri, K. Xhani, J. A. Seman, A. Trombettoni, A. Smerzi, M. Zaccanti, M. Inguscio, and G. Roati, Science **350**, 1505 (2015).

[25] A. Burchianti, F. Scazza, A. Amico, G. Valtolina, J. A. Seman, C. Fort, M. Zaccanti, M. Inguscio, and G. Roati, Phys. Rev. Lett. **120**, 025302 (2018).

[26] K. C. Wright, R. B. Blakestad, C. J. Lobb, W. D. Phillips, and G. K. Campbell, Phys. Rev. Lett. **110**, 025302 (2013).

[27] F. Jendrzejewski, S. Eckel, N. Murray, C. Lanier, M. Edwards, C. J. Lobb, and G. K. Campbell, Phys. Rev. Lett. **113**, 045305 (2014).

[28] A. C. Mathey, C. W. Clark, and L. Mathey, Phys. Rev. A **90**, 023604 (2014).

[29] K. Snizhko, K. Isaieva, Y. Kuriatnikov, Y. Bidasyuk, S. Vilchinskii, and A. Yakimenko, Phys. Rev. A **94**, 063642 (2016).

[30] S. Eckel, J. G. Lee, F. Jendrzejewski, C. J. Lobb, G. K. Campbell, and W. T. Hill, Phys. Rev. A **93**, 063619 (2016).

[31] G. Gauthier, S. S. Szigeti, M. T. Reeves, M. Baker, T. A. Bell, H. Rubinsztein-Dunlop, M. J. Davis, and T. W. Neely, arXiv:1903.04086.

[32] C. D'Errico, S. S. Abbate, and G. Modugno, Phil. Trans. R. Soc. A **375**, 20160425 (2017).

[33] J. Polo, V. Ahufinger, F. W. J. Hekking, and A. Minguzzi, Phys. Rev. Lett. **121**, 090404 (2018).

[34] J. Polo, R. Dubessy, P. Pedri, H. Perrin, and A. Minguzzi, Phys. Rev. Lett. **123**, 195301 (2019).

[35] A. Griffin, T. Nikuni, and E. Zaremba, *Bose-Condensed Gases at Finite Temperatures* (Cambridge University Press, Cambridge, England, 2009).

[36] See Supplemental Material at http://link.aps.org/supplemental/10.1103/PhysRevLett.124.045301, which includes Refs. [37–56], for details on methodology, analysis and extraction of vortex ring properties at zero and finite temperatures.
[37] A. Burchianti, G. Valtolina, J. A. Seman, E. Pace, M. De Pas, M. Inguscio, M. Zaccanti, and G. Roati, Phys. Rev. A **90**, 043408 (2014).
[38] W. Ketterle and M. Zwierlein, Riv. Nuovo Cimento **31**, 247 (2008).
[39] A. Smerzi and A. Trombettoni, Phys. Rev. A **68**, 023613 (2003).
[40] B. Jackson and E. Zaremba, Phys. Rev. A **66**, 033606 (2002).
[41] E. Goldobin, D. Koelle, R. Kleiner, and A. Buzdin, Phys. Rev. B **76**, 224523 (2007).
[42] T. Frisch, Y. Pomeau, and S. Rica, Phys. Rev. Lett. **69**, 1644 (1992).
[43] C. Raman, M. Köhl, R. Onofrio, D. S. Durfee, C. E. Kuklewicz, Z. Hadzibabic, and W. Ketterle, Phys. Rev. Lett. **83**, 2502 (1999).
[44] J. W. Park, B. Ko, and Y. Shin, Phys. Rev. Lett. **121**, 225301 (2018).
[45] J. R. Anglin, Phys. Rev. A **65**, 063611 (2002).
[46] P. Mason, N. G. Berloff, and A. L. Fetter, Phys. Rev. A **74**, 043611 (2006).
[47] A. L. Fetter, Rev. Mod. Phys. **81**, 647 (2009).
[48] R. Hänninen and A. W. Baggaley, Proc. Natl. Acad. Sci. U.S.A. **111**, 4667 (2014).
[49] C. Rorai, J. Skipper, R. M. Kerr, and K. R. Sreenivasan, J. Fluid Mech. **808**, 641 (2016).
[50] A. Villois, G. Krstulovic, D. Proment, and H. Salman, J. Phys. A **49**, 415502 (2016).
[51] R. Numasato, M. Tsubota, and V. S. L'vov, Phys. Rev. A **81**, 063630 (2010).
[52] T.-L. Horng, C.-h. Hsueh, S.-W. Su, Y.-M. Kao, and S.-C. Gou, Phys. Rev. A **80**, 023618 (2009).
[53] A. Griffin, S. Nazarenko, and D. Proment, arXiv:1910.00096.
[54] P. H. Roberts and J. Grant, J. Phys. A **4**, 55 (1971).
[55] A. J. Groszek, D. M. Paganin, K. Helmerson, and T. P. Simula, Phys. Rev. A **97**, 023617 (2018).
[56] S. Donadello, S. Serafini, M. Tylutki, L. P. Pitaevskii, F. Dalfovo, G. Lamporesi, and G. Ferrari, Phys. Rev. Lett. **113**, 065302 (2014).
[57] I. Marino, S. Raghavan, S. Fantoni, S. R. Shenoy, and A. Smerzi, Phys. Rev. A **60**, 487 (1999).
[58] M. Pigneur and J. Schmiedmayer, Phys. Rev. A **98**, 063632 (2018).
[59] M. Zaccanti and W. Zwerger, Phys. Rev. A **100**, 063601 (2019).
[60] P. W. Anderson, Rev. Mod. Phys. **38**, 298 (1966).
[61] O. Avenel and E. Varoquaux, Phys. Rev. Lett. **55**, 2704 (1985).
[62] Y. Sato and R. E. Packard, Rep. Prog. Phys. **75**, 016401 (2012).
[63] E. Hoskinson, Y. Sato, I. Hahn, and R. E. Packard, Nat. Phys. **2**, 23 (2006).
[64] C. Nore, M. Abid, and M. E. Brachet, Phys. Rev. Lett. **78**, 3896 (1997).
[65] T. W. Neely, E. C. Samson, A. S. Bradley, M. J. Davis, and B. P. Anderson, Phys. Rev. Lett. **104**, 160401 (2010).
[66] W. J. Kwon, S. W. Seo, and Y.-i. Shin, Phys. Rev. A **92**, 033613 (2015).
[67] W. Wang, R. N. Bisset, C. Ticknor, R. Carretero-González, D. J. Frantzeskakis, L. A. Collins, and P. G. Kevrekidis, Phys. Rev. A **95**, 043638 (2017).
[68] C. F. Barenghi, R. J. Donnelly, and W. F. Vinen, Phys. Fluids **28**, 498 (1985).
[69] A. Klein, I. L. Aleiner, and O. Agam, Ann. Phys. (Amsterdam) **346**, 195 (2014).
[70] L. Galantucci, A. W. Baggaley, N. G. Parker, and C. F. Barenghi, Proc. Natl. Acad. Sci. U.S.A. **116**, 12204 (2019).
[71] B. Jackson, N. P. Proukakis, C. F. Barenghi, and E. Zaremba, Phys. Rev. A **79**, 053615 (2009).
[72] A. J. Allen, E. Zaremba, C. F. Barenghi, and N. P. Proukakis, Phys. Rev. A **87**, 013630 (2013).
[73] A. J. Allen, S. Zuccher, M. Caliari, N. P. Proukakis, N. G. Parker, and C. F. Barenghi, Phys. Rev. A **90**, 013601 (2014).
[74] M. D. Reichl and E. J. Mueller, Phys. Rev. A **88**, 053626 (2013).
[75] M. J. H. Ku, B. Mukherjee, T. Yefsah, and M. W. Zwierlein, Phys. Rev. Lett. **116**, 045304 (2016).
[76] P. Scherpelz, K. Padavić, A. Rancon, A. Glatz, I. S. Aranson, and K. Levin, Phys. Rev. Lett. **113**, 125301 (2014).
[77] A. M. Mateo and J. Brand, New J. Phys. **17**, 125013 (2015).
[78] S. Serafini, L. Galantucci, E. Iseni, T. Bienaime, R. N. Bisset, C. F. Barenghi, F. Dalfovo, G. Lamporesi, and G. Ferrari, Phys. Rev. X **7**, 021031 (2017).
[79] L. Amico, G. Birkl, M. Boshier, and L.-C. Kwek, New J. Phys. **19**, 020201 (2017).
[80] Additional metadata are available at: https://doi.org/10.25405/data.ncl.11534988.